An Efficient Photon Utilization Radioisotope Thermophotovoltaic Based on Curled Reflectors

Jiyu Wang, Xiaobin Tang,* Sheng Zhao, Haoyue Deng, Chen Ji, Hongyu Wang, Yunpeng Liu, Xinyi Li, Hongbo Lu, and Zhiheng Xu*

For radioisotope thermophotovoltaic (RTPV) to produce higher output power, it is often required that the irradiance incident on the thermophotovoltaic (TPV) cell array be more uniform. However, the irradiance received by each cell of the TPV array is relatively different under the conventional cell array surround structure of RTPV, resulting in a serious overall electrical output mismatch loss and a lower output power utilization rate. Herein, an RTPV with curled reflectors optimized by finite-element method is proposed. It is shown in the simulation results that the irradiation uniformity of the cell array can reach 87.5%, the total output power reaches 88.12 W, which is 39.8% higher than that prior to optimization, and the mismatch loss is reduced by 69.2%. In addition, the impact of the reflectivity of reflectors is also targeted from the perspective of practical applications, and it can still produce higher output power than that of the conventional structure even at reflectivity as low as 70%. Ultimately, the RTPV prototype with reflectors is developed, and the electrical performance is tested to verify the effect of irradiance improvement. Herein, reflectors with positive gain for RTPV are proposed, which provides a new idea for the development of high-efficiency power supplies.

1. Introduction

With the expansion of human exploration in extreme environments, such as deep space, planetary surfaces, polar regions, and deep seas, the long-life and high-stability power supply become increasingly critical.[1–3] Radioisotope thermophotovoltaic (RTPV) with the advantage of long-term stable work is an attractive option.[4–6] RTPV has the inherent advantages of high output power density and high theoretical efficiency, which is regarded as one of the power sources with great development potential.[7] RTPV is mainly composed of radioisotope heat source,[8–11] thermo-optical conversion emitter/coating,[12–14] and TPV cell.[15–18] For RTPV systems, since the infrared light generated by the heat source and regulated by the emitter/coating is isotropic and diverges during propagation, each TPV cell receives different irradiance and has different electrical properties resulting from the photovoltaic effect. When all the cells were connected, the output power of the cell array often cannot reach the expected maximum value (defined as mismatch loss), and the output power utilization rate is also very low.[19,20] Therefore, optimizing the transport process of infrared light during energy conversion is very important to improve the irradiance uniformity of TPV arrays and the electrical output performance of the overall RTPV system.

The uniformity of irradiance received by the cell array can be effectively improved by adding a reflective cavity between the heat source and the TPV cell array. As shown in **Figure 1**, the infrared light originally scattered around is reflected and converged by the reflectors; thus, the cells in the lower irradiance area can be supplemented with more infrared light, causing the irradiance rise, and become consistent. However, much of the current research is focused on the flat reflective cavity,[21–23] and the reflectors can still be improved given the different structure of each power generation system. In addition, the ray-tracing method was mostly used in the previous studies, but the TPV system often transfers energy in the form of thermal radiation, so the method of surface-to-surface radiation heat transfer is also a feasible analytical approach.[24,25] The radioisotope heat source had specific structure and power, and establishing a 3D thermal radiation analysis framework would be more intuitive and practical. Moreover, experimental studies on the use of reflective cavities for thermophotovoltaic systems, either in terms of mechanism or effect, are limited.

In this work, based on a 1500 W radioisotope heat source, the irradiance distribution of TPV cells and its effect on RTPV performance were analyzed using the surface-to-surface radiation module. The optical and electrical properties of conventionally structured RTPV at different distances were investigated. Then, an RTPV with curved reflectors was designed, the

J. Wang, X. Tang, S. Zhao, H. Wang, Y. Liu, Z. Xu
Department of Nuclear Science and Technology
Nanjing University of Aeronautics and Astronautics
Nanjing 211106, China
E-mail: tangxiaobin@nuaa.edu.cn; xuzhiheng@nuaa.edu.cn

X. Tang, Y. Liu, Z. Xu
Key Laboratory of Nuclear Technology Application and Radiation
Protection in Astronautics
Ministry of Industry and Information Technology
Nanjing 211106, China

H. Deng, C. Ji, X. Li, H. Lu
State Key Laboratory of Space Power-Sources Technology
Shanghai Institute of Space Power-Sources
Shanghai 200245, China

The ORCID identification number(s) for the author(s) of this article can be found under https://doi.org/10.1002/ente.202201477.

DOI: 10.1002/ente.202201477

ADVANCED
SCIENCE NEWS
www.advancedsciencenews.com

Energy Technology
Generation, Conversion, Storage, Distribution
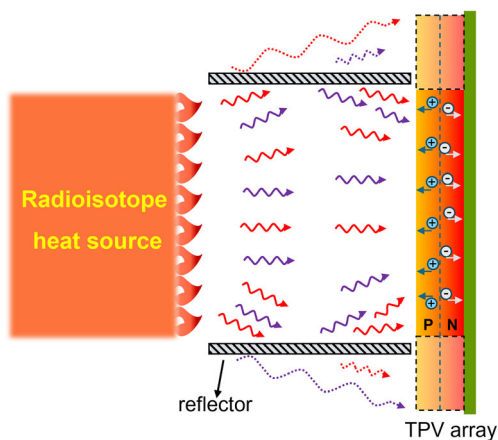www.entechnol.de

Figure 1. Schematic of radioisotope thermophotovoltaic (RTPV) with reflective cavity.

difference between irradiance and electrical output was compared and analyzed, and the optimization design scheme was provided. Subsequently, the RTPV performance under different reflector reflectivity was analyzed to evaluate the effects of potential practical situations. Finally, an RTPV prototype based on the reflector was developed, and the output enhancement effect brought by the optimization was verified.

2. Experimental Section

2.1. Characteristics of RTPV Components

Figure 2 shows the schematic of the $^{238}PuO_2$ radioisotope heat source and its coating. Six heat sources were stacked vertically for higher input energy. The innermost layer of each heat source was four $^{238}PuO_2$ pellets, each with a radius of 13.75 mm and a height of 27.5 mm, providing a thermal power of 62.5 W. The outermost layers were made of graphite, with a length of 72.33 mm, a width of 72.33 mm, and a height of 36.16 mm. The thermo-optic
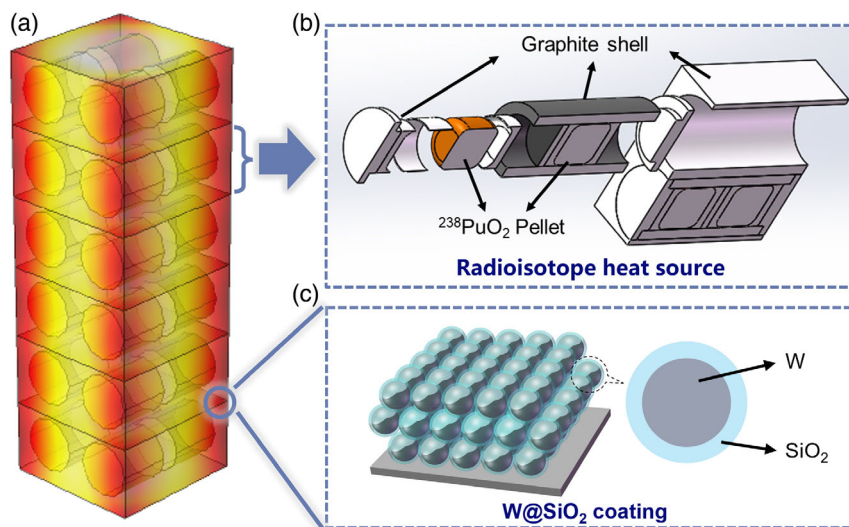
performance of the heat source was regulated by the W@SiO$_2$ coating investigated in our previous works.[14] The thickness of the coating was generally from nano - micro levels.

Figure 3a shows the emissivity of W@SiO$_2$, which has an average emissivity of 0.93 before 1800 nm and 0.13 after 1800 nm. InGaAs-based TPV cells were selected as photoelectric conversion devices. The dimension of each InGaAs cell was 10×10 mm^2, and the thickness was 1 mm. Figure 3b shows the quantum efficiency and reflectivity of the InGaAs cell, as measured by a spectral response/quantum efficiency meter (Enlitech QE-R). The response band of the InGaAs cell was 300–1800 nm, the external quantum efficiency (EQE) was over 70% in the band of 500–1600 nm, and the corresponding average reflectivity was about 5%.

2.2. Finite-Element Analysis

The temperature of the radioisotope heat source and the irradiance distribution received by the TPV arrays were obtained by COMSOL software. In steady state, the surface-to-surface radiative heat-transfer model was used for multi-physics-coupled analysis. After setting the initial thermal power, the heat source temperature and the irradiance received by the TPV arrays can be established as follows

$$\rho C_p u \times \nabla T + \nabla q = Q \qquad (1)$$

$$J = \varepsilon \times E_b + R \times G \qquad (2)$$

where ρ is the density of each device material, C_p is the specific heat at constant pressure, u is the velocity, T is the temperature, q is the heat flux, Q is the heat, J is the radiosity, ε is the emissivity, E_b is the total emissive power of blackbody radiation, R is the reflectivity, and G is the irradiance received by the TPV cell.

The emissivity of the W@SiO$_2$ coatings is a wavelength-dependent function $\varepsilon(\lambda)$ that can be accurately simulated in COMSOL using multiple spectral bands. Therefore, the emissive power P_E can be expressed as
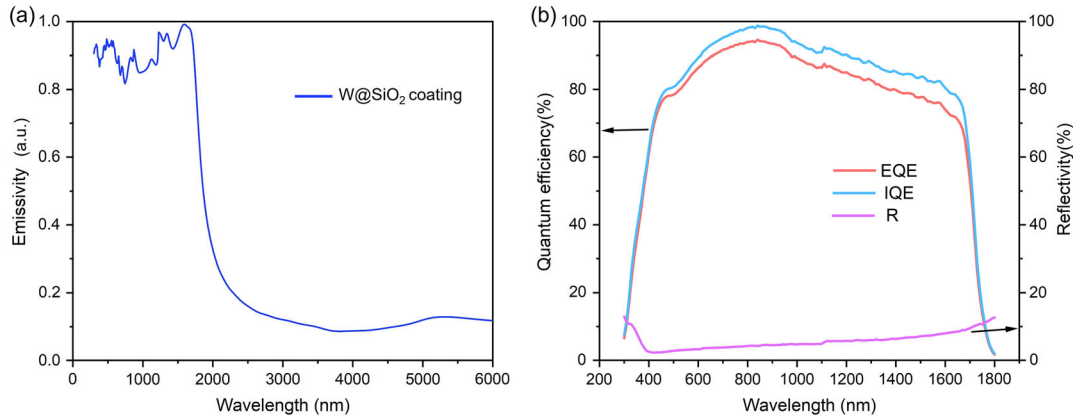

Figure 2. Schematic of a) six stacked heat sources, b) single heat source, and c) W@SiO$_2$ coating.

**ADVANCED
SCIENCE NEWS**

www.advancedsciencenews.com

Energy Technology
Generation, Conversion, Storage, Distribution

www.entechnol.de

Figure 3. a) Emissivity of the W@SiO$_2$ coating, b) external quantum efficiency (EQE), internal quantum efficiency (IQE), and reflectivity (R) of the InGaAs cell.

$$P_E = \varepsilon(\lambda)E_b(\lambda, T) = \int \frac{2\pi hc^2 \cdot \varepsilon(\lambda)}{\lambda^5} \times \frac{1}{e^{\frac{hc}{\lambda kT}} - 1} d\lambda \tag{3}$$

where h is Planck's constant, c is the speed of light in the free space, λ is the wavelength, and k is the Boltzmann constant.

The infrared light emitted by the heat source would be dissipated after a certain distance. Thus, the irradiance received by the TPV arrays was uneven to a certain extent, and a parameter N is defined to quantitatively describe the uniformity of the irradiance, as follows

$$N = 1 - \frac{\max|G_i - G_{av}|}{G_{av}} \times 100\% \tag{4}$$

where G_i is the irradiance of the ith cell, and G_{av} is the average value of the irradiance over the whole array.

The domain heat source was used to simulate the heating of ^{238}PuO$_2$ pellets, and the six stacked heat sources provided a total thermal power of 1500 W. The top and bottom of the heat source were set as adiabatic boundary conditions to obtain higher temperature with limited thermal power. Since the TPV cells can be effectively cooled by fins, heat pipe, and liquid cooling,[26] the temperature of the TPV cells was set to 300 K. The emissivity ($\varepsilon(\lambda)$) of W@SiO$_2$ coating and the reflectivity (R) of InGaAs cell were used for detailed modeling.

2.3. Electrical Properties of the RTPV

The current–voltage (I–V) characteristic curves of the TPV cells can be calculated according to the Shockley diode equation as follows

$$I(V) = I_{sc} - I_0 \left[\exp\left(\frac{e \cdot V}{kT_c} \right) - 1 \right] \tag{5}$$

$$P = I \times V \tag{6}$$

where I is the output current, I_{sc} is the short-circuit current, I_0 represents the reverse saturation current, e is the charge amount, V is the output voltage, T_c is the cell temperature, and P is the electrical output power. I_{sc} can be calculated by the following formula

$$I_{sc} = \int_0^\infty \frac{2\pi ec}{\lambda^4} \cdot EQE(\lambda) \cdot \varepsilon(\lambda) \cdot \frac{1}{e^{\frac{hc}{\lambda kT}} - 1} d\lambda \tag{7}$$

where $EQE(\lambda)$ is the EQE of the TPV cell. When the TPV cell is at a certain distance from the heat source, and the irradiance is different, the I_{sc} becomes

$$I'_{sc} = \frac{G}{\varepsilon e_b(\lambda, T)} \left[I_{sc,ref} + \alpha(T_c - T_{c,ref}) \right] \tag{8}$$

where $I_{sc,ref}$ is the output current at the reference irradiance ($\varepsilon e_b(\lambda, T)$) and the reference cell test temperature ($T_{c,ref}$), α is the relative temperature coefficient of the output current. $T_{c,ref}$ usually choses 300 K, which is the same as the cell preset temperature (T_c), so I'_{sc} can be simplified to be

$$I'_{sc} = \frac{G}{\varepsilon e_b(\lambda, T)} I_{sc,ref} \tag{9}$$

Combining the previous equations, the I–V characteristic curves of all TPV cells can be obtained. When the TPV cells use series arrays to generate electricity, the mismatch loss can be expressed as

$$\text{Mismatch Loss} = P_{mpp,sum} - P_{mpp,array} \tag{10}$$

where $P_{mpp,sum}$ is the sum of the output power of each cell at the maximum power point (MPP), $P_{mpp,array}$ indicates the output power at MPP when all the cells are connected in series.

The process of output analysis of TPV array is shown in **Figure 4**. First extract the irradiance data of TPV cells from COMSOL software, and then use python software to obtain the average irradiance of the corresponding area according to the size of each cell. Finally, the electrical output characteristics of the TPV array were obtained from Equation (5)–(10).
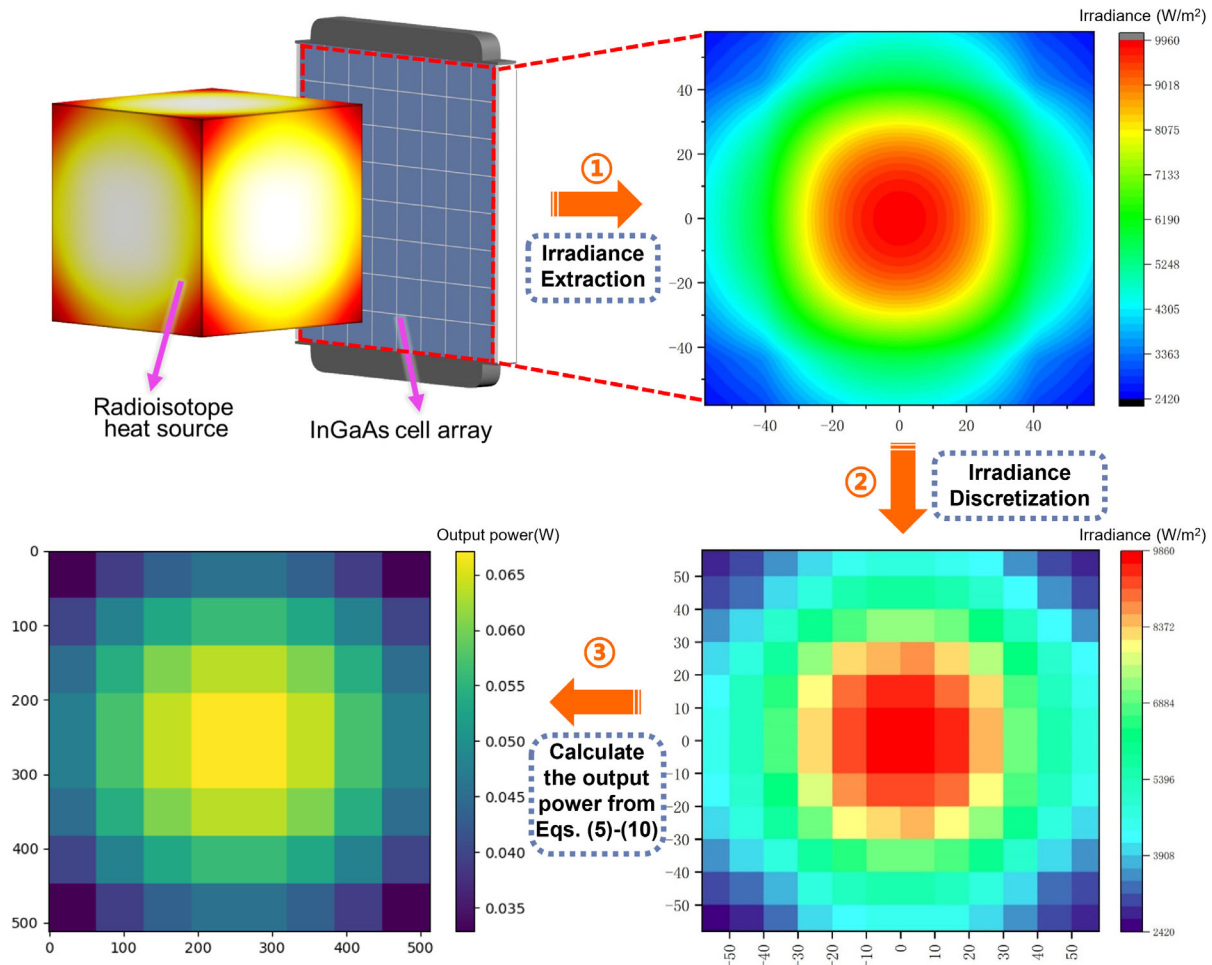
Figure 4. The process of TPV array output analysis.

3. Results and Discussion

3.1. Performance of the Conventional Cell Array Surround Structure RTPV

As shown in **Figure 5**a, the radioisotope heat sources were in the center, InGaAs cell arrays were arranged in parallel around them, and the heat sinks were attached to the back of the cell arrays to control the temperature. Figure 5b shows the thermal radiation power spectra of the heat sources regulated by the W@SiO$_2$ coating, and the illustration shows the temperature distribution on the lateral surface of the heat sources. The lateral surface temperature of the heat source can reach more than 1200 K, and the temperature difference on the lateral surface could be controlled within 10 K, so the average temperature can effectively reflect the temperature characteristics of the heat source.[27]

To study the variation of irradiance under the conventional cell array surround structure of RTPV, the height of the InGaAs cell array was fixed at 21 cm, the distance between cell array and heat source was set at 2–12 cm, the width of the cell array was correspondingly varied in the range of 10–30 cm, and the corresponding changes in the number of cells were shown in Table S1,

Supporting Information. As shown in **Figure 6**, when the distance was 2 cm, the high-irradiance area of the InGaAs cell array was highly coincident with the projected area of the heat source, and the irradiance difference between the center and the edge of the array was the most evident. As the distance increases, the area of the InGaAs cell array becomes larger, and the infrared light emitted from other lateral surfaces of the heat source can also be received. Therefore, the area with higher irradiance gradually becomes an elliptical shape, and the transition from high irradiance to low irradiance becomes more gradual.

The irradiance uniformity and mismatch loss of the InGaAs cell array are shown in **Figure 7**. The irradiance uniformity increased with distance, and the increase was more obvious after the distance of 7 cm. The mismatch loss decreases with distance and is 17.11 W at 2 cm and 8.14 W at 12 cm, mainly due to the corresponding increase in irradiance from 46.8% to 55.7%. However, the mismatch loss value is above 8 W, with an average of 11 W, even close to the output power of the array (the I–V and power–voltage (P–V) curves of the series array are shown in Figure S1, Supporting Information). The main reason is that the irradiance uniformity of the array is insufficient (maintain in the range of 45–56%). The cells at the edge of the array
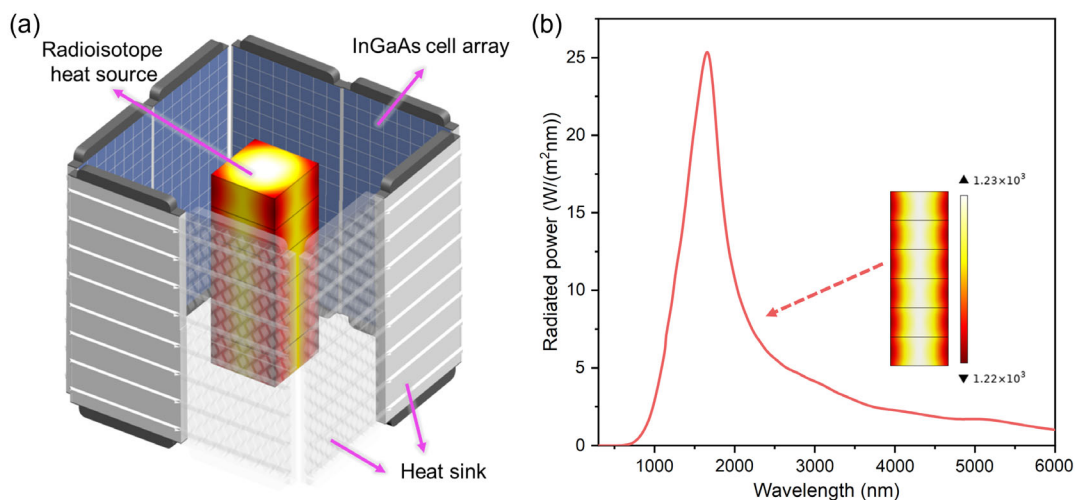
ADVANCED
SCIENCE NEWS
www.advancedsciencenews.com

Energy Technology
Generation, Conversion, Storage, Distribution
www.entechnol.de

Figure 5. a) Schematic of the conventional cell array surround RTPV, and b) thermal radiation power spectra and lateral surface temperature distribution of heat source.
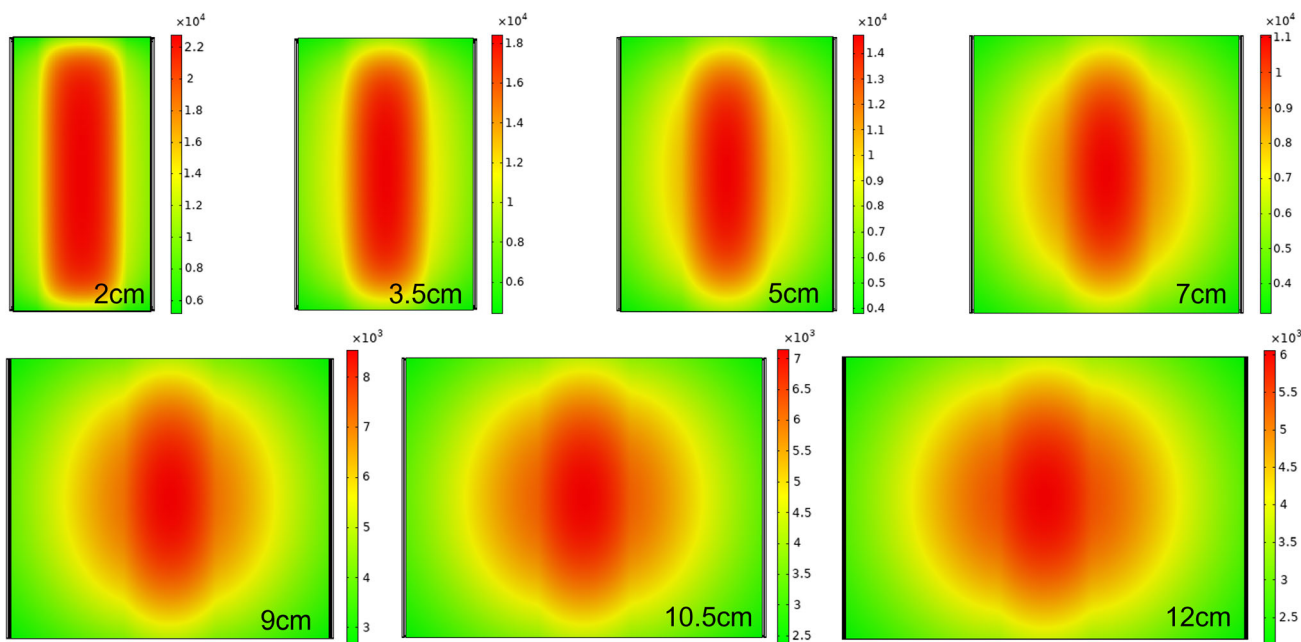

Figure 6. Irradiance distribution of InGaAs cell array at different distances from the heat source.

generate less current due to the low irradiance they receive, while the output current of the array is determined by them, leading to an increase in array losses. Therefore, although better irradiance uniformity would result in lower mismatch losses, the effect by increasing the distance is very limited.

3.2. RTPV Performance with Optimized Design Reflectors

RTPV with curled reflectors were designed and compared with that of flat reflectors, and their schematic diagrams are shown in **Figure 8**a,b. As the conventional cell array surround structure of RTPV, the cell array was still arranged in parallel with the heat

source, but the array width was narrowed, and the vertically placed reflectors were added at the edge of the cell array. When the infrared light emitted by the heat source is incident on the reflector, part of it is reflected onto the cells, which substantially improves the irradiance uniformity of the cell array. The cross section of RTPV with reflectors is shown in Figure 8c. To maximize the utilization of the limited space and reduce light leakage, the size parameters have the following relationship

$$l_h/2 + d_{cell} = l_{cell}/2 + l_F(l_C) \qquad (11)$$

where l_h is the width of heat source, d_{cell} is the distance between the heat source and the cell array, l_{cell} is the width of cell array, l_F is

ADVANCED
SCIENCE NEWS
www.advancedsciencenews.com

Energy Technology
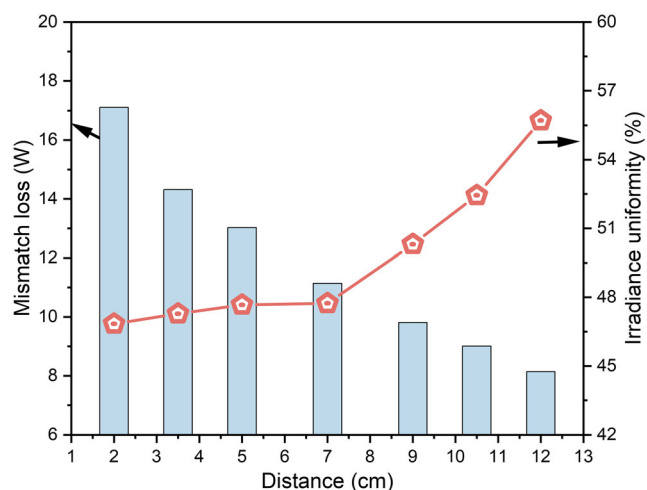Generation, Conversion, Storage, Distribution
www.entechnol.de

Figure 7. Irradiance uniformity and mismatch loss of the InGaAs cell array at different distances.

the length of flat reflector, and l_C is the chord length of curved reflector. Since the curved reflector is tangent to the dotted line inclined at 45° in Figure 8c, it can be seen from the geometric relationship in Figure 8d that the cross section of the curved reflector is a 1/4 circle, and its central angle is 90°. Therefore, the diameter d_C of the entire circle corresponding to the curved reflector section is $\sqrt{2}$ times of l_C. To reserve sufficient space for the reflectors and make the volume of RTPV relatively small, d_{cell} is set to 7 cm. l_{cell} varies from 7 to 10 cm, and other components and structural parameters are unchanged.

Different reflector lengths and array widths greatly influence the reflection effect, and width ratio was adopted to quantitatively analyze the influence of these two parameters, which is defined as follows

$$\text{width ratio} = \frac{l_{cell}}{l_{cell} + 2 \times l_C} \tag{12}$$

It represents the ratio of the array width with reflector to the original array width, and the value varied in the range of 35–50%
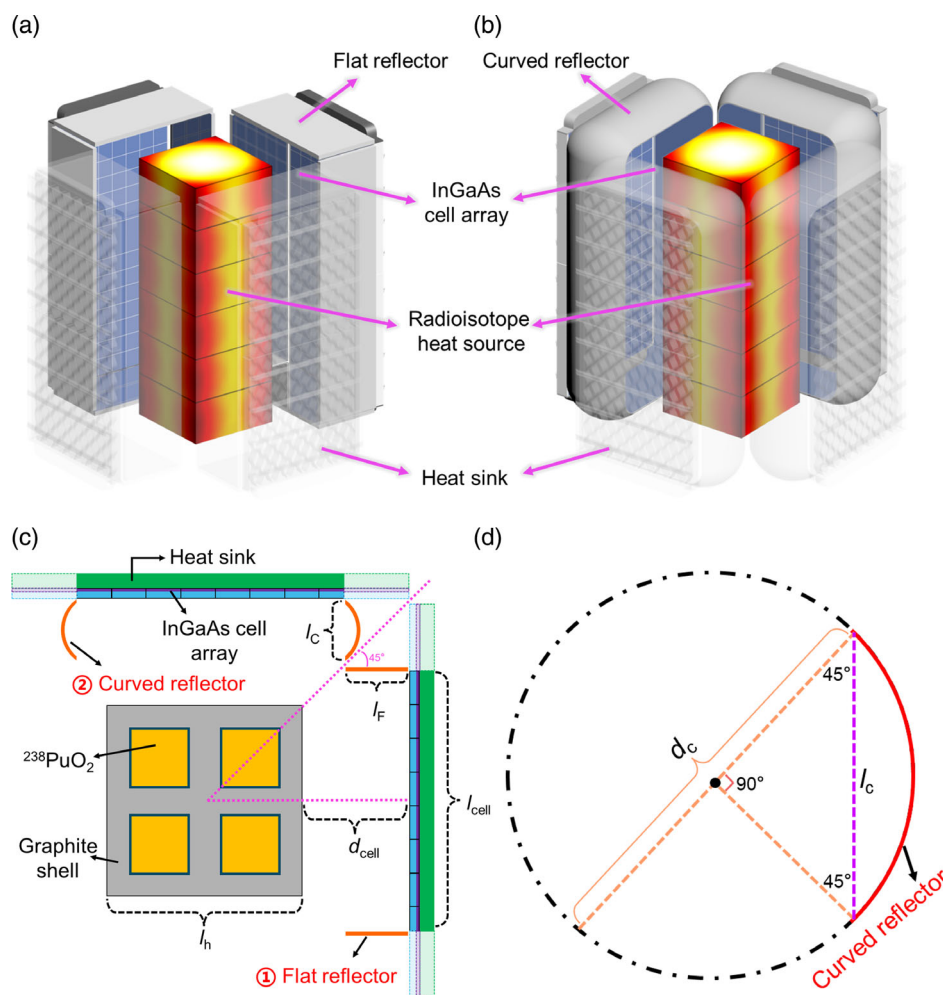

Figure 8. Schematic of RTPV with a) flat reflectors and b) curled reflectors, c) cross-sectional diagram of RTPV with reflectors, and d) geometric parameters of curved reflector section.

ADVANCED
SCIENCE NEWS

www.advancedsciencenews.com

Energy Technology
Generation, Conversion, Storage, Distribution

www.entechnol.de

(the number of cells in each case is shown in Table S2, Supporting Information). As shown in **Figure 9**, with different reflectors and different width ratios, the irradiance of InGaAs cell array with reflectors was significantly improved, compared with the conventional cell array surround structure of RTPV. The irradiance of an array with a width ratio of 35% is more concentrated, more evenly distributed, and numerically higher due to the wider reflector reflecting more divergent infrared light. Compared with the flat reflectors, the curved reflectors allow more of the reflected infrared light to reach the edge of the array, thereby obtaining higher irradiance in the edge area.

Figure 10a shows the irradiance uniformity of the cell array at different width ratios, and the shaded area in the figure is the irradiance uniformity range under the conventional cell array surround structure of RTPV (without reflector). The irradiance uniformity with flat reflectors remains around 80%, whereas that of the curved reflectors exceeds 85% and reaches a maximum of 87.5% when the width ratio is 35%, which is evidently better than that case without reflector. Figure 10b shows the maximum output power of the array in series ($P_{mpp,array}$) with different width ratios. The curved reflector leads to higher $P_{mpp,array}$, which is 1.72 W higher than the flat reflector on average at different width ratios, due to the effect of irradiance uniformity. The $P_{mpp,array}$ produced by the cell array without reflector is only in the range of 10–12 W, which is about half of that with reflectors.

The irradiance distribution diagrams along the horizontal and vertical symmetry axes of the array are shown in Figure 10c,d. The irradiance difference under the curled reflectors is the smallest, and the horizontal difference is 0.27 W cm^{-2}, which is 0.3 and 0.1 W cm^{-2} lower than that without reflector and that of flat reflectors, respectively. The vertical difference of irradiance is slightly larger because the vertical height of the array has not been changed, and the difference caused by the curled reflectors is 0.35 W cm^{-2}, which is 0.12 and 0.15 W cm^{-2} lower than the two other cases. Therefore, the improvement of irradiance uniformity mainly occurs in the horizontal direction. Figure 10e shows the I–V curves of the InGaAs cell array. The short-circuit current of the array caused by curved reflectors is 0.533 A, which is 9.5% higher than that of flat reflectors and nearly five times higher than that caused by conventional structure without reflector. The array in the conventional configuration has higher open voltage (closer to 140 V) due to the larger number of cells, but its effect is not as great as the short-circuit current, so the higher output power of InGaAs cell arrays with curved reflectors is mainly due to higher short-circuit current. The power mismatch and power density of the array are shown in Figure 10f. The power mismatch caused by the curved reflectors is the smallest at 3.43 W, which is 30% of the conventional structure without reflector; and the power density is the largest at 149.85 mW cm^{-2}, which is 5.7 times than that without reflector. Therefore, the total output power and the system efficiency of RTPV can reach 88.12 W and 5.87%, respectively, which is due to the better irradiance uniformity generated by the curved reflectors. The RTPV with curved reflectors relies on better emission spectra and higher temperature of heat source to further improve the conversion efficiency, and the related research results are shown in Figure S2, Supporting Information.
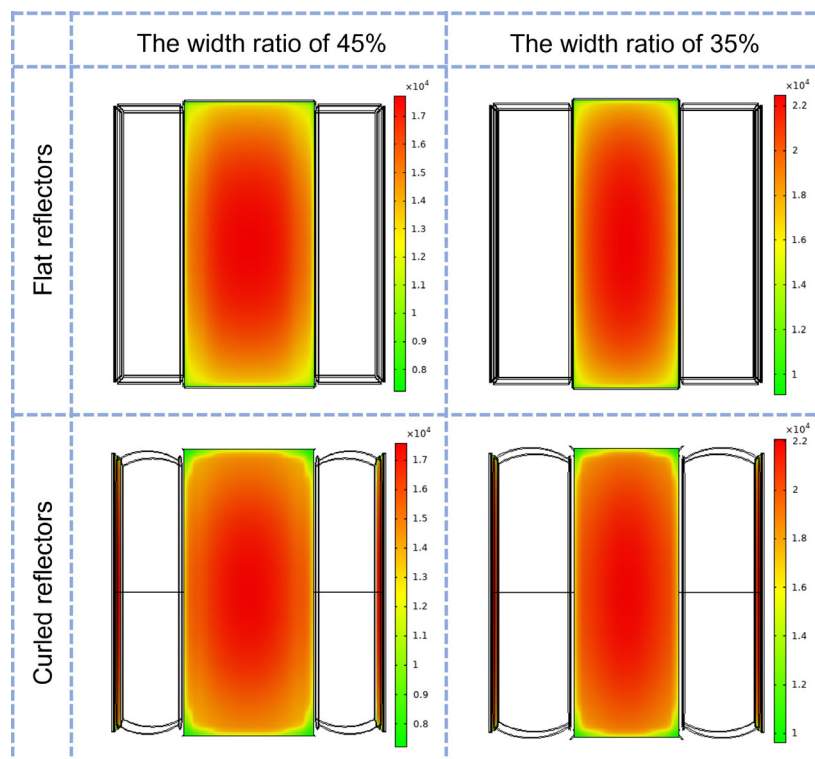

Figure 9. Irradiance of the cell array at width ratios of 45% and 35% with flat reflectors and curled reflectors, respectively.
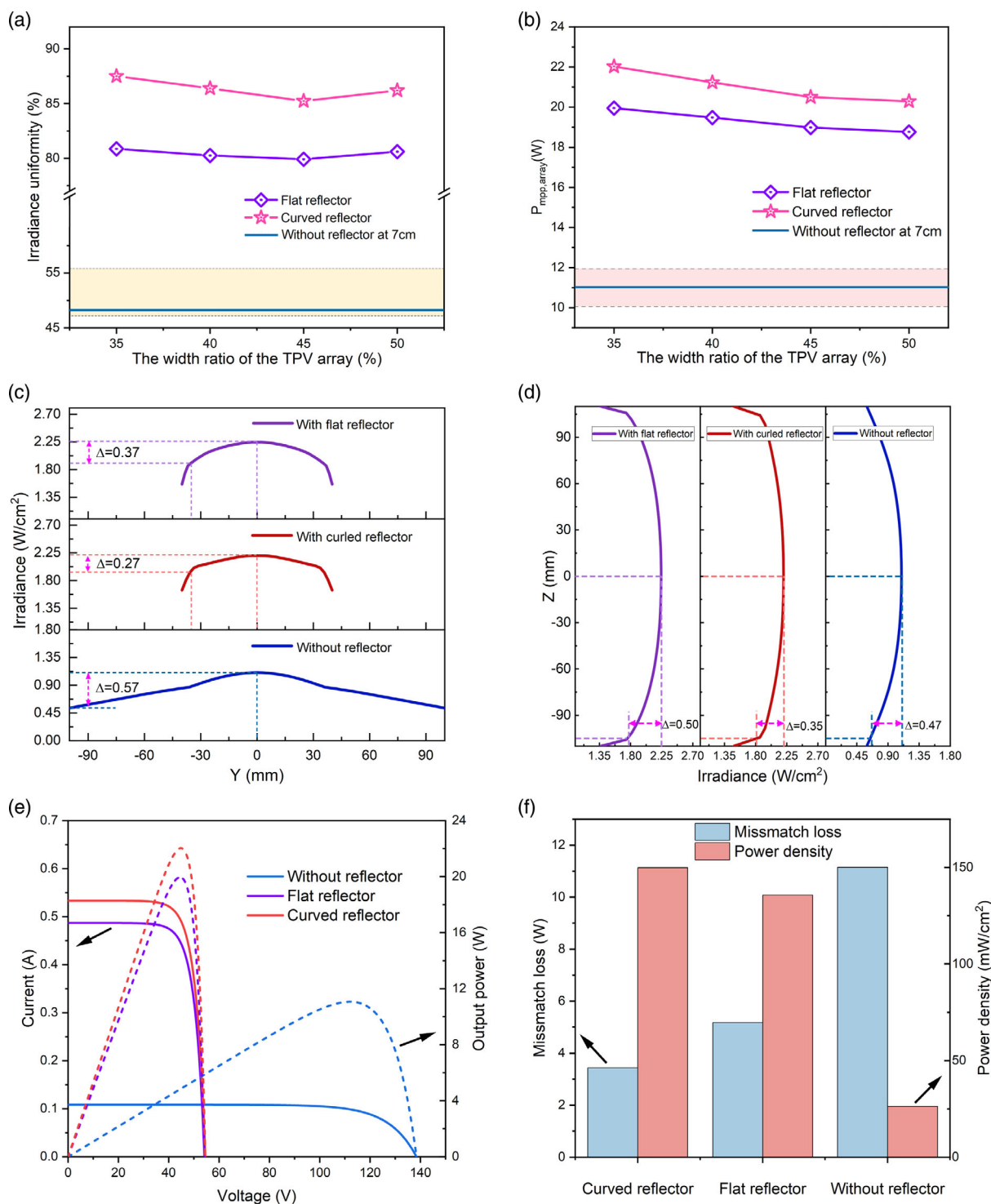
Figure 10. a) Irradiance uniformity and b) $P_{mpp,array}$ of RTPV with reflectors at different array width ratios (the shaded area is the range of data without reflector). Irradiance profiles along the c) horizontal and d) vertical symmetry axes, e) current–voltage (I–V) curves, f) mismatch loss, and power density of the cell array at the width ratio of 35%, and the corresponding data without reflector are listed for comparison.

3.3. Optimized RTPV with Different Reflector Reflectivity

Figure 11a shows the irradiation uniformity and output power of the cell array when the reflectivity of the curved reflector decays

in the range of 70–95%. The irradiance uniformity decreases with the decrease in reflectivity, but generally remains above 80%, which is still better than that of the flat reflectors. The illustrations are the irradiance distribution diagrams of the cell array
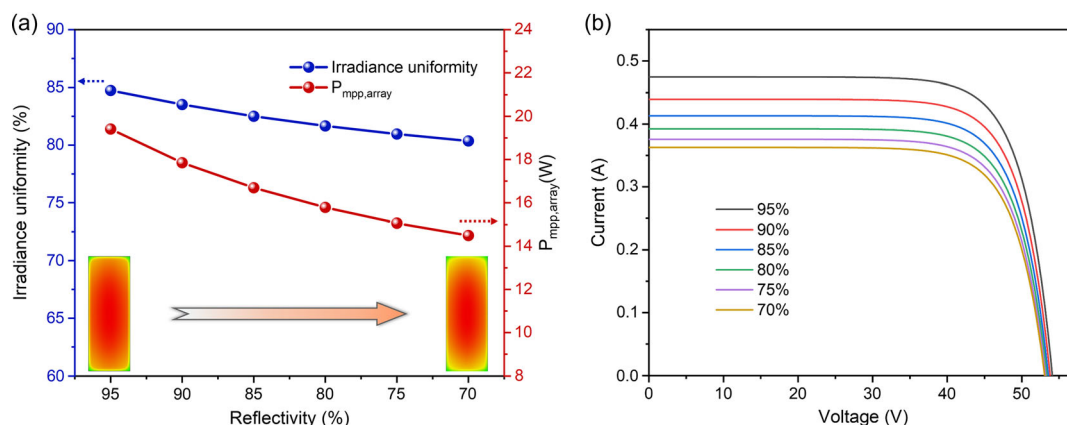
ADVANCED
SCIENCE NEWS
www.advancedsciencenews.com

Energy Technology
Generation, Conversion, Storage, Distribution
www.entechnol.de

Figure 11. a) Irradiance uniformity and $P_{\text{mpp,array}}$, b) I–V curves of the array under the influence of different reflectivity of the curved reflector when the width ratio is 35%.

when the reflectivity is 95% and 70%, which clearly show that the difference in irradiance between the central area and the peripheral area increases, corresponding to the variation in irradiance uniformity. The $P_{\text{mpp,array}}$ of the cell array also decreases as the reflectivity decreases. The main reason is that the reflector with lower reflectivity absorbs more irradiance, thereby reducing the intensity and uniformity of irradiance reflected to the cell array. As a result, the short-circuit current of the array decreases. The corresponding I–V curves of the cell array are shown in Figure 11b. Nonetheless, the $P_{\text{mpp,array}}$ of the array is 14.5 W at the reflectivity of 70%, which is still 3.44 W higher than that without reflector at the same distance. In addition, existing commercial reflectors can achieve a reflectivity of more than 90% in a wideband, and even up to 95%.[28] Therefore, curved reflectors can substantially increase the practical application potential of the RTPV.

3.4. Effectiveness Verification Test of RTPV Prototype with Reflector

Figure 12 shows the RTPV prototype and its test equipment, and an electric-heating column was used to simulate a radioisotope-fuel pellet for experimental research. The power of the heat-source column was provided by a programmable linear DC power supply (DP832A, RIGOL Technologies Inc.), and the input electric power varied from 10 to 30 W. The InGaAs cell was fixed on the RTPV shell, which was 3.5 cm away from the heat source. A water-cooling temperature control module was placed under the RTPV prototype to ensure the low temperature of the entire shell and InGaAs cell through heat conduction. The reflectors were made with a highly reflective thin-film aluminum mirror (MIRO-SILVER 27-4270AG, Alanod–Solar) with a total light reflection of 98% (Figure S3, Supporting Information). One part
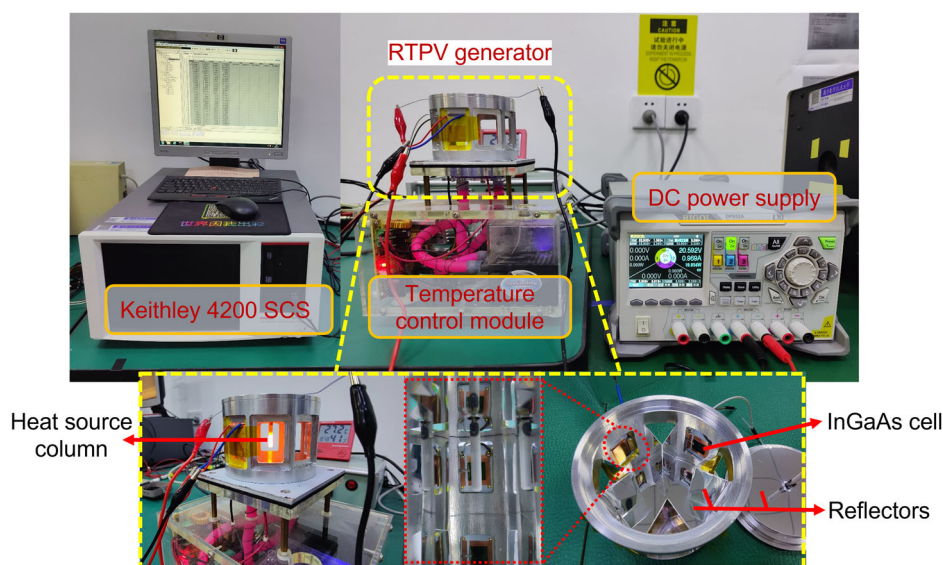

Figure 12. RTPV prototype and experiment.

**ADVANCED
SCIENCE NEWS**

www.advancedsciencenews.com

Energy Technology
Generation, Conversion, Storage, Distribution

www.entechnol.de

of the reflectors was vertically placed on the side of the InGaAs cell (occupying the window where the cell was originally placed), and the other part was placed on the top and bottom of the RTPV prototype. The electrical performance of the RTPV was tested by a parameter analyzer (Keithley 4200 SCS) at a temperature of 300 K and an atmospheric pressure of 1 atm.

The electrical characteristics of the RTPV prototype under different electrical input power are shown in **Figure 13**. In all cases, the RTPV with reflector produces significantly higher output current and power. When the electric input power was 30 W, the I_{sc} and P_{max} of the RTPV prototype with reflectors were 26.24 mA and 1.63 mW, which are 1.70 times and 1.73 times higher than those without reflector, respectively. The results strongly indicate that the RTPV prototype with reflector can converge infrared light and enhance its intensity.

The output improvement of InGaAs cell was difficult to be reflected at different positions on the receiving surface due to the space limitation of RTPV prototype housing. Thus, a larger

standard blackbody radiation source was used for testing, as shown in **Figure 14**. The temperature of the standard blackbody radiation source (DEMEI, DY-HT3 Blackbody Furnace) was set to 1250 K, and the temperature of the InGaAs cell was controlled at 295 K. The exit aperture of the blackbody source was 4 cm, and the reflector was selected as a square with a side length of 5 cm. According to the distribution diagrams of infrared light taken on a white screen at a distance of 5 cm from the standard blackbody radiation source in the dark environment, and considering the symmetry of infrared light distribution, four different positions (A, B, C, and D) were selected for measurement, and the remaining test conditions were unchanged.

Figure 15 shows the I_{sc} and P_{max} of the InGaAs cell at the four tested positions. The output current and power increased significantly after adding the reflector, and the corresponding $I/P–V$ curves are shown in Figure S4, Supporting Information. The I_{sc} of the InGaAs cell at positions B and C was higher than the measured data at position A, this is because that more
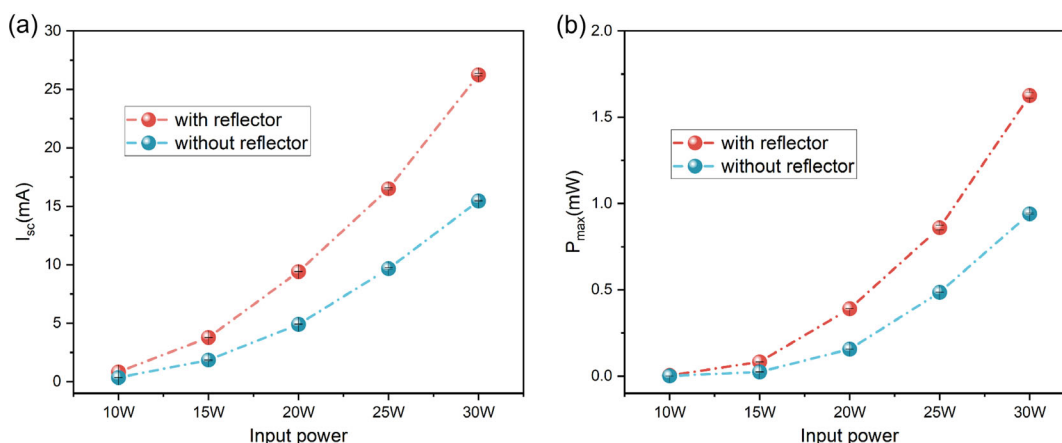

Figure 13. a) Short-circuit current (I_{sc}) and b) P_{max} of RTPV prototype with and without reflector.
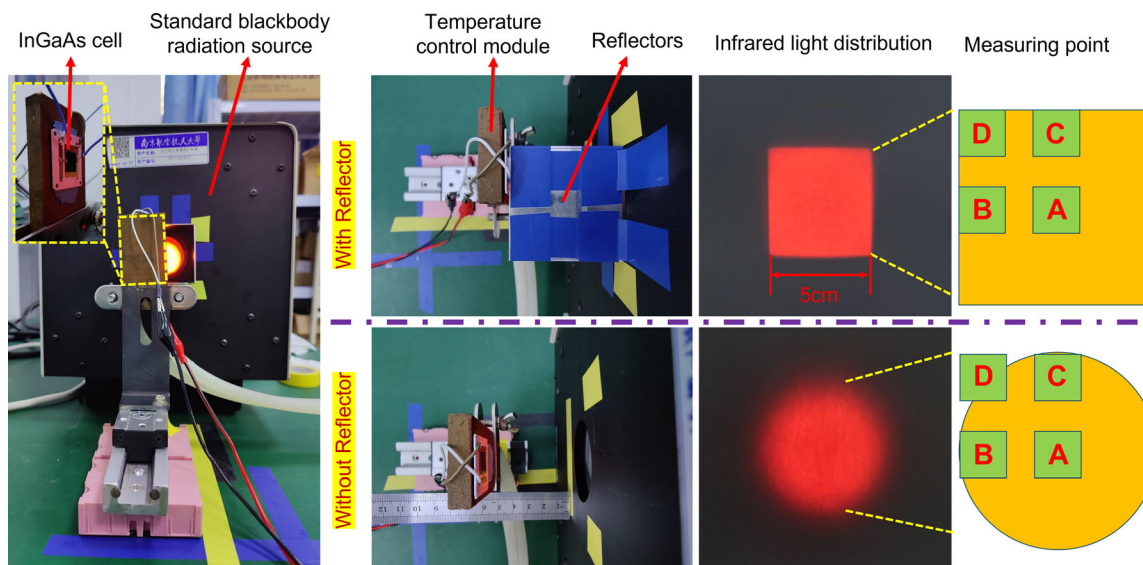

Figure 14. Test scenario of InGaAs cell under standard blackbody radiation source.

**ADVANCED
SCIENCE NEWS**

www.advancedsciencenews.com

Energy Technology
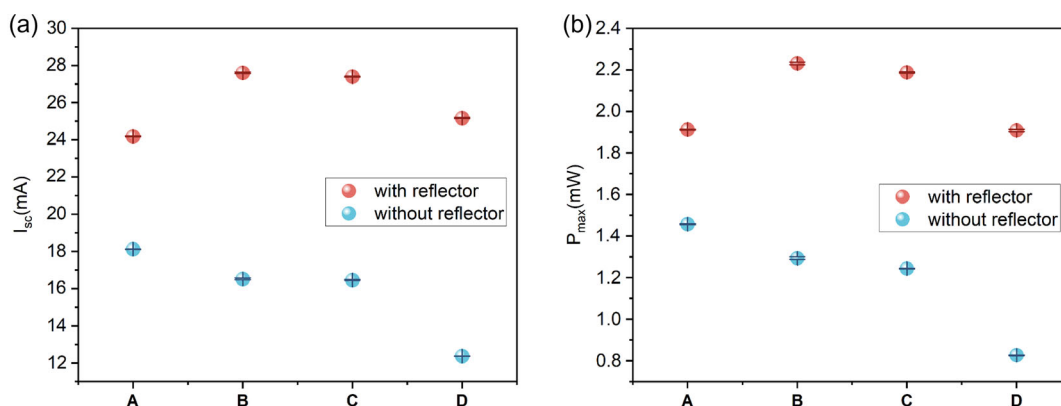Generation, Conversion, Storage, Distribution

www.entechnol.de

Figure 15. a) I_{sc} and b) P_{max} of InGaAs cell at different positions in RTPV prototype with and without reflector.

infrared light was reflected to these two regions and forming high-irradiance areas (similar irradiance simulation results can also be observed in ref. [23]). Moreover, I_{sc} is positively correlated with the irradiance received by the cell according to Equation (9), which ultimately results in the highest electrical output of InGaAs cell at positions B and C. At position D, the output of InGaAs cell has the largest increase, with I_{sc} increasing from 12.37 to 25.17 mA and P_{max} increasing from 0.83 to 1.91 mW, presenting an increase by more than two times. The results reveal that the reflector can significantly increase the irradiance in the previously low-irradiance area, even exceeding the central position A. Therefore, the RTPV with reflector can improve the irradiance uniformity and electrical output, and the effect is consistent with the simulation results. We believe that the irradiance uniformity and electrical output performance of the prototype will be more significantly improved, if a full-size RTPV prototype is established with an output array consisting of multiple TPV cells connected in series.

4. Conclusion

To improve the irradiance uniformity of RTPV, a curled reflector was designed and the irradiance distribution characteristics of the cell array under the influence of radioisotope heat source were analyzed by finite-element method. When the width ratio of the reflector was 35%, the irradiance uniformity of a cell array was increased to 87.5%, the mismatch loss was reduced to 3.43 W, the power density could reach 149.85 mW cm^{-2}, and the total output power of RTPV reached 88.12 W. Compared with the conventional structure without reflector, the irradiance uniformity and $P_{mpp,array}$ of the proposed structure increased by 39.8% and 47.7 W, respectively, and the mismatch loss was reduced by 69.2%. Furthermore, the RTPV with curled reflectors can still maintain a good electrical output at a low reflector reflectivity, and it still produces higher power than the conventional structure without reflector even when the reflectivity is 70%. The experimental results also prove that the reflector can positively improve the output power and irradiance of RTPV. These results strongly prove the superiority and feasibility of applying the reflector to RTPV, and this work provides an

alternative reference scheme for reducing the mismatch loss and improving output power utilization rate of RTPV.

Supporting Information

Supporting Information is available from the Wiley Online Library or from the author.

Conflict of Interest

The authors declare no conflict of interest.

Data Availability Statement

The data that support the findings of this study are available from the corresponding author upon reasonable request.

[1] X. Wang, R. Liang, P. Fisher, W. Chan, J. Xu, *Renew. Sustain. Energy Rev.* **2020**, *119*, 109572.
[2] Mazzetti As, M. Gianotti Pret, G. Pinarello, L. Celotti, M. Piskacev, A. Cowley, *Acta Astronaut.* **2019**, *156*, 162.

[3] J. Herrera, S. Sierra, A. Ibeas, *J. Mar. Sci. Eng.* **2021**, *9*, 356.

[4] A. Datas, A. Martí, *Sol. Energy Mater. Sol. Cells* **2017**, *161*, 285.

[5] M. A. Prelas, C. L. Weaver, M. L. Watermann, E. D. Lukosi, R. J. Schott, D. A. Wisniewski, *Prog. Nucl. Energy* **2014**, *75*, 117.

[6] C. Ferrari, F. Melino, M. Pinelli, P. R. Spina, *Appl. Energy* **2014**, *113*, 1717.

[7] T. Burger, C. Sempere, B. Roy-Layinde, A. Lenert, *Joule* **2020**, *4*, 1660.

[8] R. G. Lange, W. P. Carroll, *Energy Convers Manag* **2008**, *49*, 393.

[9] A. Schock, M. Mukunda, C. Or, V. Kumar, G. Summers, *Acta Astronaut.* **1995**, *37*, 21.

[10] J. Lee, S. Cheon, S. Hong, Y. Nam, *Int. J. Heat Mass. Transfer.* **2017**, *108*, 1115.

[11] S. J. Cheon, S. G. Hong, J. H. Lee, Y. S. Nam, *Int. J. Energy Res.* **2018**, *42*, 817.

[12] I. Celanovic, F. O'Sullivan, M. Ilak, J. Kassakian, D. Perreault, *Opt. Lett.* **2004**, *29*, 863.

[13] K. A. Amedome Min-Dianey, H. C. Zhang, N. L. P. M'Bouana, C. Su, X. Xia, *Energy* **2018**, *154*, 488.

[14] C. Meng, Y. Liu, Z. Xu, H. Wang, X. Tang, *Energy* **2022**, *239*, 121884.

[15] M. M. A. Gamel, H. J. Lee, W. E. S. W. A Rashid, P. J. Ker, L. K. Yau, M. A. Hannan, Md. Z. Jamaludin, *Materials (Basel)* **2021**, *14*, 4944.

[16] D. Fan, T. Burger, S. McSherry, B. Lee, A. Lenert, S. R. Forrest, *Nature* **2020**, *586*, 237.

[17] A. LaPotin, K. L. Schulte, M. A. Steiner, K. Buznitsky, C. C. Kelsall, D. J. Friedman, E. J. Tervo, R. M. France, M. R. Young, A. Rohskopf, S. Verma, E. N. Wang, A. Henry, *Nature* **2022**, *604*, 287.

[18] B. Roy-Layinde, T. Burger, D. Fan, B. Lee, S. McSherry, S. R. Forrest, A. Lenert, *Sol. Energy Mater. Sol. Cells* **2022**, *236*, 111523.

[19] T. Bauer, *Thermophotovoltaics: Basic Principles and Critical Aspects of System Design*, Springer Science & Business Media **2011**, https://doi.org/10.1007/978-3-642-19965-3, ISSN 1865-3529, ISBN 978-3-642-19964-6.

[20] P. F. Baldasaro, M. W. Dashiell, J. E. Oppenlander, J. L. Vell, P. Fourspring, K. Rahner, L. R. Danielson, S. Burger, E. Brown, *AIP Conf. Proc.* **2004**, *61*, 738.

[21] C. Zhang, L. Tang, Y. Liu, Z. Liu, W. Liu, K. Qiu, *Energy* **2020**, *195*, 116962.

[22] G. Saraey, J. Gholami, A. Gharehghani, A. M. Dehghani, *Sol. Energy* **2022**, *231*, 1115.

[23] X. L. Liu, X. Chen, X. L. Li, X. L. Xia, S. C. Liu, Y. Liu, *Energy Technol.* **2022**, *10*, 1.

[24] T. Zhou, Z. Sun, S. Li, H. Liu, D. Yi, *Energies* **2016**, *9*, 772.

[25] A. H. Kazim, A. Salman, A. B. Khan, U. Shaukat, A. Shabbir, *J. Energy Resour. Technol. Trans. ASME* **2022**, *144*, 1.

[26] H. M. S. Bahaidarah, A. A. B. Baloch, P. Gandhidasan, *Renew. Sustain. Energy Rev* **2016**, *57*, 1520.

[27] É Fontana, L. Battiston, R. G. A. Oliveira, C. A. Capeletto, L. F. L. Luz, *Energy* **2022**, *239*.

[28] M. Alnajideen, G. Min, *Energy Convers. Manag.* **2022**, *251*, 114981.